**Citation: Molecular Therapy—Nucleic Acids (2016) 5, e357;** doi:10.1038/mtna.2016.72
Official journal of the American Society of Gene & Cell Therapy
www.nature.com/mtna

# $^{18}$F-FDG PET/CT for Monitoring the Response of Breast Cancer to miR-143-Based Therapeutics by Targeting Tumor Glycolysis

**Ying Miao[1], Ling-fei Zhang[2,3], Rui Guo[1], Sheng Liang[4], Min Zhang[1], Shuo Shi[1], Cheng-fang Shang-Guan[1], Mo-fang Liu[2,3] and Biao Li[1]**

**Increased glucose utilization is a hallmark of cancer, and tumor metabolism is emerging as anticancer target for therapeutic intervention. Triple-negative breast cancers TNBC are highly glycolytic and show poor clinical outcomes. We previously identified hexokinase 2, the major glycolytic enzyme, as a target gene of miR-143 in TNBC. Here, we developed a therapeutic formulation using *cholesterol-modified miR-143 agomir* encapsulated in a neutral lipid-based delivery agent that blocked tumor growth and glucose metabolism in TNBC tumor-bearing mice when administered systemically. The antioncogenic effects were accompanied by a reduction in the direct target hexokinase 2 and [$^{18}$F]-fluorodeoxyglucose ($^{18}$F-FDG) uptake based on positron emission tomography/computed tomography. Treatment with miR-143 formulation has minimal toxic effects and mice tolerated it well. Thus, we demonstrated that miR-143 is a robust inhibitor of the Warburg effect and an effective therapeutic target for TNBC. In addition, $^{18}$F-FDG positron emission tomography/computed tomography can be used to specifically monitor the response of TNBC to miR-143-based therapeutics by targeting tumor glycolysis.**

*Molecular Therapy—Nucleic Acids* (2016) **5**, e357; doi:10.1038/mtna.2016.72; published online 30 August 2016
**Subject Category:** miRNAs, siRNAs and shRNAS

## Introduction

Breast cancer is the most common malignancy in women worldwide and the leading cause of female cancer death in less developed countries.[1] Roughly 15–20% of all breast cancer cases fall into the category of triple-negative breast cancer (TNBC), which is characterized by a lack of gene expression for the estrogen receptor, progesterone receptor, and human epidermal growth factor receptor 2 (ref. 2).Clinical studies have indicated that patients with TNBC after neoadjuvant and/or adjuvant chemotherapy show significantly higher recurrence rates and worse prognosis, with a median survival of ~ 1 year following treatment.[3] Unfortunately, no genomic target of proven therapeutic utility against TNBC has been identified,[4] primarily due to the exceptional gene expression.

Metabolic reprogramming is one of the hallmarks of cancer cells.[5] Even in the presence of oxygen, tumor cells preferentially rely on glycolysis, rather than oxidative phosphorylation, for ATP generation. This metabolic anomaly is commonly referred to as the "Warburg effect" (aerobic glycolysis),[6] which leads to faster glucose metabolism in cancer cells and can be used for tumor visualization with [$^{18}$F]-fluorodeoxyglucose ($^{18}$F-FDG) positron emission tomography/computed tomography (PET/CT) scanning. This method relies on the rapid glucose consumption of tumor tissue and has broad clinical applications, including assisting in the detection, staging, and evaluation of prognosis of tumors, as well as monitoring the tumor response to therapy.[7,8] Members of the hexokinase family catalyze the first committed and irreversible step of glucose metabolism, which governs the direction and magnitude of glucose flux.[9] Hexokinase 2 (HK2), the major isozyme of the hexokinase family, shows significantly elevated expression in many tumor types compared with normal cells, suggesting its potential as a metabolic target for cancer therapy.[10]

MicroRNAs (miRNAs) are a class of short (~22 nt) endogenous RNAs involved in the modulation of a diverse range of biological processes by regulating the stability and translation of their target mRNAs.[11,12] miR-143, which is downregulated in multiple cancers ranging from colorectal to breast cancers, acts as an antioncomir.[13–16] We previously found that HK2 is a direct target of miR-143[16], which may play an important role in tumor defense. However, further studies are necessary to determine whether the therapeutic delivery of miR-143 to target tumor tissues can be efficiently achieved and to monitor its treatment efficacy by using a noninvasive method.

In this study, we demonstrated that chemically synthesized miR-143 mimic suppressed glycolysis by downregulating HK2 in MDA-MB-231 cells, as well as regulated the proliferative, migrative, and apoptotic behavior of TNBC cells. Systemic delivery of miR-143 agomir to TNBC xenografts dramatically reduced both tumor growth and $^{18}$F-FDG uptake based on PET/CT. Our results demonstrate that miR-143 is a robust inhibitor of the Warburg effect and a

[1]Department of Nuclear Medicine, Ruijin Hospital, Shanghai Jiaotong University School of Medicine, Shanghai, China; [2]Center for RNA Research, State Key Laboratory of Molecular Biology-University of Chinese Academy of Sciences, Institute of Biochemistry and Cell Biology, Shanghai Institutes for Biological Sciences, Chinese Academy of Sciences, Shanghai, China; [3]Shanghai Key Laboratory of Molecular Andrology, Institute of Biochemistry and Cell Biology, Shanghai Institutes for Biological Sciences, Chinese Academy of Sciences, Shanghai, China; [4]Department of Nuclear Medicine, Xinhua Hospital, Shanghai Jiaotong University School of Medicine, Shanghai, China. Correspondence: Biao Li, Department of Nuclear Medicine, Ruijin Hospital, Shanghai Jiaotong University School of Medicine; 197 Ruijin Er Road, Shanghai 200025, China. E-mail: lb10363@rjh.com.cn.
Received 5 July 2016; accepted 18 July 2016; published online 30 August 2016. doi:10.1038/mtna.2016.72

promising therapeutic target for TNBC treatment. In addition, $^{18}$F-FDG PET/CT exhibits great potential for specifically monitoring the response of TNBC to miR-143-based therapeutics by targeting tumor glycolysis.

## Results

### miR-143 suppresses glycolysis by targeting HK2

We first analyzed the rate of glycolysis using glucose and lactate assay kits and then measured $^{18}$F-FDG uptake of MDA-MB-231 cells transfected with miR-143 mimic to evaluate its effect on glycolysis. Following treatment with miR-143 mimic, the cells exhibited decreased rates of glucose consumption and lactate production, indicating that the glycolytic pathway was repressed (**Figure 1a**). In addition, *in vitro* dynamic $^{18}$F-FDG uptake assays revealed that the miR-143 mimic-treated cells exhibited a significantly lower level of $^{18}$F-FDG uptake than control cells (**Figure 1b**). Furthermore, we evaluated the expression of HK2, which may play a pivotal role in glycolysis. Treatment with miR-143 mimic decreased both HK2 mRNA expression and protein levels in MDA-MB-231 cells (**Figure 1c**,**d**). These findings demonstrate that miR-143 targets HK2 and exerts an inhibitory effect on glycolysis in TNBC cells.

### miR-143 inhibits cell growth, migration, and induces apoptosis

The results of previous studies have supported the role of miR-143 as a tumor suppressor.[22,23] Indeed, we found that introduction of miR-143 significantly inhibited the proliferation and migration of MDA-MB-231 cells (**Figure 2a**,**b**). Flow cytometry assay also demonstrated enhanced cell apoptosis following miRNA treatment (**Figure 2c**). Collectively, these results confirmed that miR-143 could suppress proliferation and migration while inducing apoptosis in TNBC cells.

### Systemic delivery of miR-143 agomir effectively restrained tumor growth in TNBC tumor-bearing mice

Next, we investigated whether the tumor suppressive function of miR-143 intervention in TNBC cells could be reproduced in a tumor-bearing mice model. Once the tumor diameter reached ~ 5mm, a cholesterol-modified and Cy3-labeled miR-143 oligo (miR-143 agomir) encapsulated in a neutral lipid-based delivery vehicle was introduced intravenously once every 3 days over a total period of 15 days ($n$ = 3) (**Figure 3a**). Two control groups that separately received Cy3-labeled miRNA agomir control (Ctrl RNA agomir) or phosphate-buffered saline (PBS) were also established. Successful administration of miRNA agomir was confirmed by the detection of localized Cy3 signals in the tumors of both mice injected with miR-143 agomir and those receiving Ctrl RNA agomir (**Figure 3d**, left upper panels). As shown in **Figure 3b**, the time course of tumor growth indicated that systemic delivery of miR-143 agomir effectively inhibited tumor growth compared with Ctrl RNA agomir group. This was supported by tumor volume measurements (**Figure 3c**). Immunohistochemical staining revealed dramatic upregulation of the cell apoptosis marker caspase-3 and downregulation of the cell proliferation marker proliferating cell nuclear antigen in tumor tissues obtained from miR-143 agomir group compared with in Ctrl RNA agomir group (**Figure 3d**, right panels).Taken together, these results demonstrate the therapeutic efficacy of miR-143 against TNBC tumors.

### $^{18}$F-FDG PET/CT in monitoring response to miR-143-based therapy in TNBC xenografts

The mice bearing TNBC xenografts were further subjected to $^{18}$F-FDG microPET/CT scans every 5 days during the course of treatment (**Figure 3a**). No statistically significant difference in the mean or maximum tumor uptake of $^{18}$F-FDG in the treatment group was observed prior to the administration of miR-143 agomir compared with the negative control group (baseline, Day 0. **Figure 4a**,**b**). After treatment for 15 days, however, the mean standardized uptake value (SUVmean) derived from the tumor uptake of $^{18}$F-FDG was decreased by 33% in miR-143 agomir group compared with in the group that received Ctrl RNA agomir as quantified by regions of interest analysis (**Figure 4b**, right panel). Furthermore, the post-treatment $^{18}$F-FDG SUVmean was 36% lower than the tumor uptake at baseline in miR-143 agomir group (**Figure 4b**, right panels). Similarly, the post-treatment maximum standardized uptake value (SUVmax) in the treatment group showed a 43% decrease compared with the negative control group and a 31% decrease compared with the pretreatment baseline level (**Figure 4b**, left panel). Interestingly, we observed increased mean and maximum tumor uptake of $^{18}$F-FDG in mice receiving miR-143 agomir on day 5, followed by a sharp decrease of both values on days 10 and 15 compared with both control groups (**Figure 4a**,**b**). Additionally, $^{18}$F-FDG microPET/CT imaging confirmed that tumor growth in miR-143 agomir mice was markedly inhibited compared with in the negative control group (**Figure 4a**). Moreover, both immunohistochemical staining and western blotting indicated significantly lower levels of HK2 in tumors subjected to miR-143 agomir treatment compared with in controls (**Figure 4c**,**d**). In conclusion, $^{18}$F-FDG PET/CT, a noninvasive monitoring technique, is feasible for estimating the clinical response to miR-143-based targeting tumor metabolism therapy.

### Toxicity assessment of miR-143-based therapy

To assess the potential toxicity of miR-143-based therapy in a longer observed term, another three randomized groups of TNBC tumor-bearing xenografts were established ($n$ = 3 mice in each group). Encapsulated miRNA agomirs or PBS was administered intravenously every 3 days for 10 cycles. The observed time was prolonged to 30 days, while the other therapeutic conditions remained unchanged. The toxicity assessment was mainly performed by monitoring the body weights of the mice every 3 days and performing clinical chemical tests on their blood samples collected on day 30. As anticipated, no behavioral change or significant body weight loss was observed throughout the course of treatment (**Figure 5a**). miR-143 formulation caused a slight increase in serum urea (**Figure 5b**), and the levels of hemoglobin, platelets, and red blood cells counts in miR-143 agomir group showed a mild decline (**Figure 5b**), when compared with both control groups. Serum levels of alanine aminotransferase and aspartate aminotransferase liver enzymes as well as total cholesterol were slightly elevated (**Figure 5b**), while the numbers of white blood cells were mildly decreased in both treatment group and negative control group (**Figure 5b**),

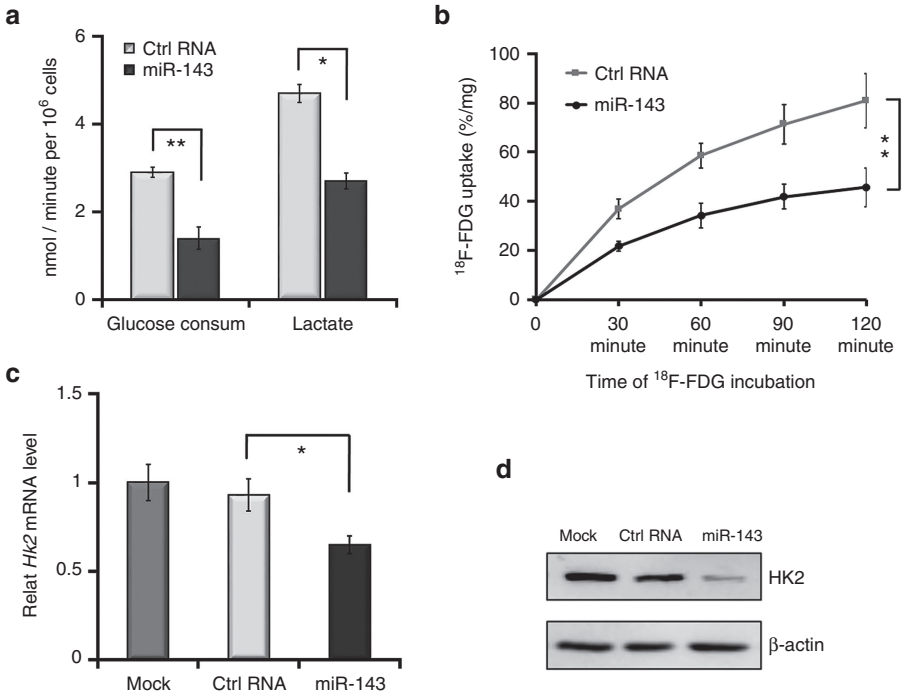


**Figure 1 miR-143 represses glycolysis by targeting hexokinase 2 (HK2) in MDA-MB-231 cells.** (**a**) Following transfection with RNA oligonucleotides (miR-143 mimic or Ctrl RNA) and incubation in low-glucose medium, the glucose metabolism rates of MDA-MB-231 cells were detected using specialized kits. The left panel shows the rates of glucose consumption, while the right panel shows the rates of lactate production. (**b**) miR-143 repressed [$^{18}$F]-fluorodeoxyglucose ($^{18}$F-FDG) uptake of MDA-MB-231 cells in an *in vitro* dynamic $^{18}$F-FDG uptake assay. (**c**) miR-143 downregulated the mRNA level of HK2 in quantitative reverse-transcriptase-polymerase chain reaction (qRT-PCR). Mock represents the phosphate buffered saline (PBS) group. (**d**) miR-143 inhibited protein expression of HK2 as evident by western blotting. Values represent the mean ± SD of three separate experiments. *$P$ < 0.05, **$P$ < 0.01, ***$P$ < 0.001.

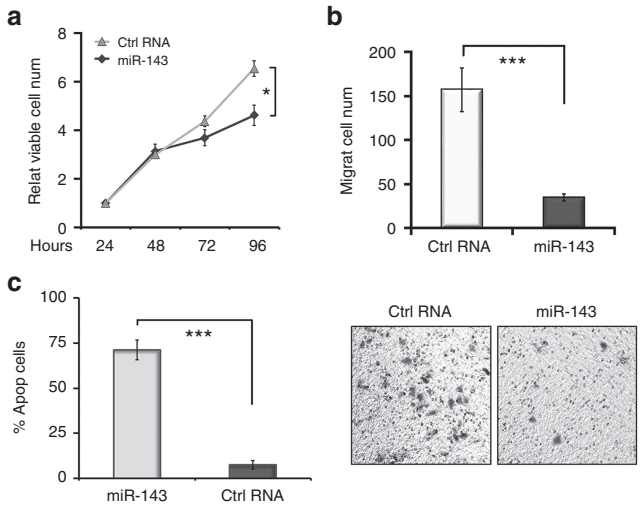


**Figure 2 miR-143 regulates the proliferation, migration, and apoptosis of MDA-MB-231 cells.** (**a**) miR-143 inhibited the proliferation activity of MDA-MB-231 cells in MTT assays. (**b**) miR-143 effectively suppressed cell migration in Transwell migration assays. (**c**) miR-143 significantly induced cell apoptosis in flow cytometry assays. Values represent the mean ± SD of three separate experiments. *$P$ < 0.05, **$P$ < 0.01, ***$P$ < 0.001.

when compared with PBS group. But all the values remained within normal ranges. Taken together, these results reveal that miR-143 treatment at the dosage and frequency as used in our study showed minimal toxic effects on the tested animals. The slight change in levels of liver enzymes, total cholesterol and white blood cells counts appear to be related to the chemistry of agomir and delivery agent rather than miR-143.

To further explore the biodistribution of Cy3-labeled miR-143 delivery mediated by neutral lipid-based agents to other organs, sections of the heart, lung, brain, liver, kidney, spleen, and muscle were examined for fluorescence. There was significant miRNA agomir uptake and cytoplasmic distribution in the liver and kidney (**Figure 5c**). Moderate miRNA agomir uptake was observed in heart and muscle (**Figure 5c**). There was a small amount of uptake in the spleen, while faint fluorescence was distributed in the brain and lung (**Figure 5c**).

## Discussion

The finding that cancer cell proliferation benefits from accelerated glucose metabolism has prompted intense research efforts aimed at developing therapeutic agents that target and selectively suppress certain glycolytic enzymes. It has been hypothesized that the best inhibitory effect can be achieved by stopping glucose flux during the initial steps of glycolysis in cancer cells, which would, in theory, disrupt all downstream steps and metabolic intermediates that support tumor anabolic processes. In this regard, hexokinase, which converts a 6-carbon sugar molecule to the corresponding hexose phosphate, appears to be an attractive

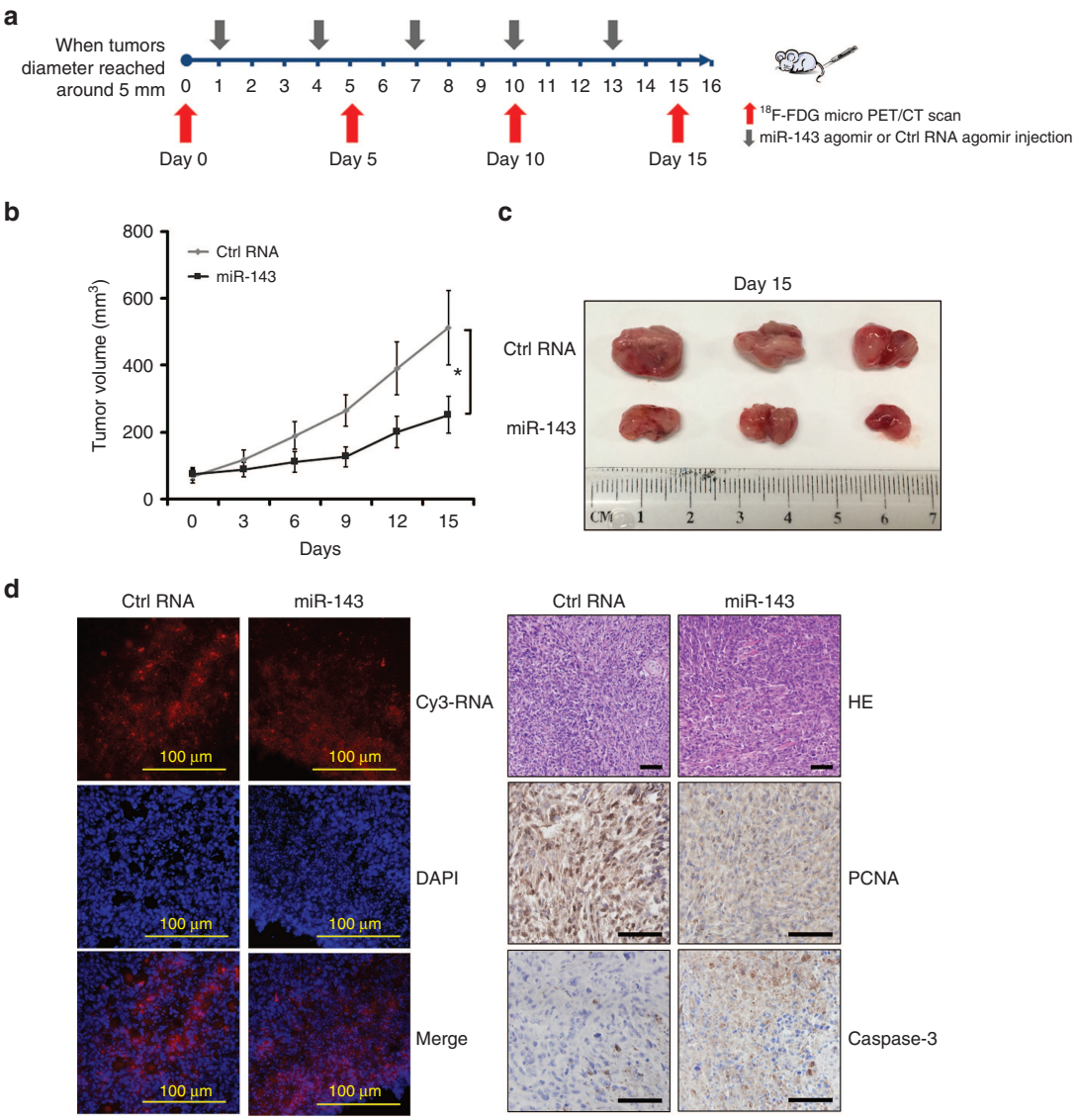


**Figure 3 Systemic delivery of miR-143 agomir inhibits tumor growth in mouse models of triple-negative breast cancer (TNBC).** (**a**) Schematic diagram of the experimental design. For this experiment, 6–8-week-old female BALB/c athymic nude mice were used for subcutaneous xenografts. When tumor diameters reached ~ 5 mm, Cy3-labeled miR-143 agomir (treatment group) or Cy3-labeled Ctrl RNA agomir (negative control group) encapsulated in a lipid-based delivery vehicle was administered through tail vein injections at 1.5 mg/kg of body weight every 3 days for 5 cycles. (**b**) Time course of TNBC tumor growth in mice treated with miR-143 agomir or Ctrl RNA agomir. (**c**) Tumors were resected from miR-143 agomir and Ctrl RNA agomir mice. (**d**) Cy3 signals were detectable in tumor tissue slices from Cy3-labeled miRNA agomir shown in the upper left panels. Nucleus counterstained with 4′,6-diamidino-2-phenylindole on tumor tissue slices are shown in the middle left panels. The merged images are shown in the lower left panels. Immunohistochemical staining is presented in the right panels and included hematoxylin and eosin (HE), proliferating cell nuclear antigen (PCNA) (brown), and caspase-3 (brown) detection of TNBC tumor sections from the 2 groups. Scale bars: 100 μm. All data are mean ± SD of three separate experiments. *$P < 0.05$, **$P < 0.01$, ***$P < 0.001$. $n = 3$ in each group.

target for cancer therapy. Indeed, an increasing number of studies has linked oncogenesis with HK2 overexpression, which serves as a key mediator of aerobic glycolysis and promotes tumor growth.[24,25] Supporting this notion, Nissim Hay *et al.* demonstrated that systemic deletion of HK2 in mouse models reduced the tumor burden of nonsmall cell lung cancer and breast cancer, suggesting the possibility of targeting HK2 for treatment of breast cancer.[26] Previously, we observed a significant inverse correlation between HK2 mRNA and miR-143 levels in breast cancer patients, which lent further evidence that miR-155/miR-143 cascade was involved in the control of glycolysis by regulating HK2 expression in breast cancer cells.[16] The interaction between miR-143 and HK2 was also verified in several other types of cancers, including colon cancer, lung cancer, head and neck squamous cell carcinoma, among others.[17–20,27] Despite these advances, systemic delivery of formulated miR-143 as a glycolysis inhibitor for cancer therapy has not been reported. Moreover, the therapeutic evaluation of miRNA by molecular imaging remains relatively unexplored.

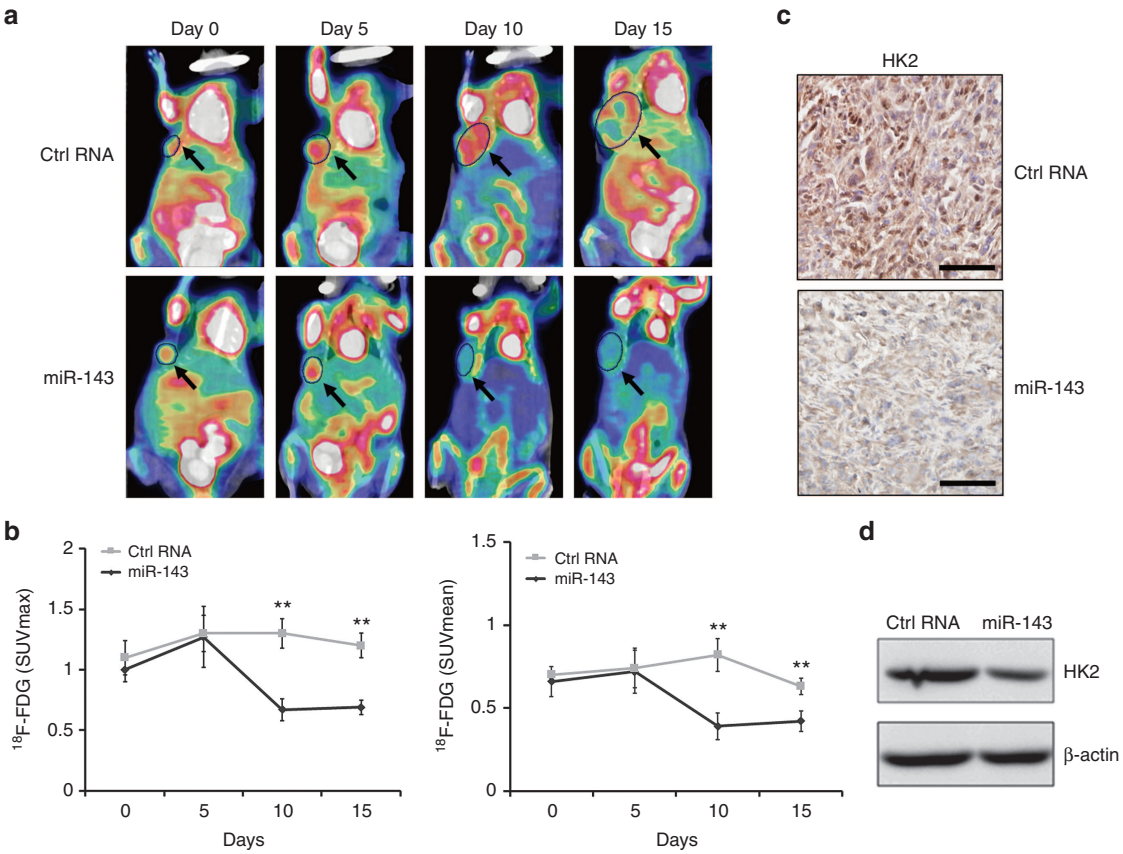


**Figure 4 Assessment of response to miR-143-based therapy in triple-negative breast cancer (TNBC) xenografts.** (**a**) [$^{18}$F]-fluorodeoxyglucose ($^{18}$F-FDG) microPET/CT imaging of mice treated with miR-143 agomir or Ctrl RNA agomir at days 0 (baseline), 5, 10, and 15. Representative $^{18}$F-FDG micro positron emission tomography/computed tomography (PET/CT) images are shown with circles indicating xenografted TNBC tumors. (**b**) Quantification of tumor uptake of $^{18}$F-FDG is presented as maximum standardized uptake value (SUVmax) and mean standardized uptake value (SUVmean). (**c**) Hexokinase2 (HK2) expression of TNBC tumor sections from immunohistochemical staining. (**d**) HK2 protein levels determined by western blotting. All data are mean ± SD of three separate experiments. $^{*}P < 0.05$, $^{**}P < 0.01$, $^{***}P < 0.001$.

The results described herein demonstrated for the first time that intravenous delivery of miR-143 agomir with a lipid-based formulation effectively inhibited glycolysis and the growth of xenografted TNBCs. This study was performed through systemic administration, by which effective drug distribution to primary tumors can be achieved and is closely related to the clinical pathway. For miRNA-based therapeutic application, chemical modifications of oligonucleotides together with an efficient delivery system are required. Accordingly, we employed a chemically synthesized and cholesterol-modified miRNA agomir encapsulated into a neutral lipid-based delivery reagent to achieve higher stability and more robust penetration into target tissues. Moreover, in contrast to siRNAs or shRNAs, which generally modulate a single transcript, miRNAs may simultaneously target multiple cancer-related pathways, leading to stronger clinical benefits.[28] Besides ERK5, TLR2, and N-RAS among others, HK2 was verified as one of the oncogenes subjected to miR-143 regulation in this study.[22,29,30] Collectively, miR-143 appears to be a strong target candidate for antitumor therapeutics.

$^{18}$F-FDG PET/CT has been extensively explored in a wide range of basic research and clinical applications, ranging from the cellular and molecular mechanisms that determine $^{18}$F-FDG uptake to the well-documented utility in multiple diseases, particularly in cancer. In this study, we evaluated the feasibility of using $^{18}$F-FDG PET/CT scanning to monitor the efficacy of miR-143-based therapies. We demonstrated that five cycles of intravenous administration of miR-143 agomir significantly reduced tumor uptake of $^{18}$F-FDG (SUVmean and SUVmax) compared with both the pretreatment baseline and the value found in mice treated with Ctrl RNA agomir. Our findings in animal models were further corroborated by immunohistochemical staining and western blotting, both of which demonstrated that HK2 was suppressed in the presence of miR-143, supporting the conclusion of a recent study that HK2 is an independent predictor of $^{18}$F-FDG uptake.[31] Consistent with previous findings indicating that a correlation exists between $^{18}$F-FDG uptake and cellular proliferation, the rate of growth in miR-143 agomir-treated tumors was decreased compared with controls, accompanied by the downregulation of proliferating cell nuclear antigen observed at the end of treatment. However, this correlation was not observed in the late period of the treatment, during which tumor growth continued; however, $^{18}$F-FDG uptake decreased and the SUVmean value decreased more sharply in the negative control group. These opposing trends may be attributed

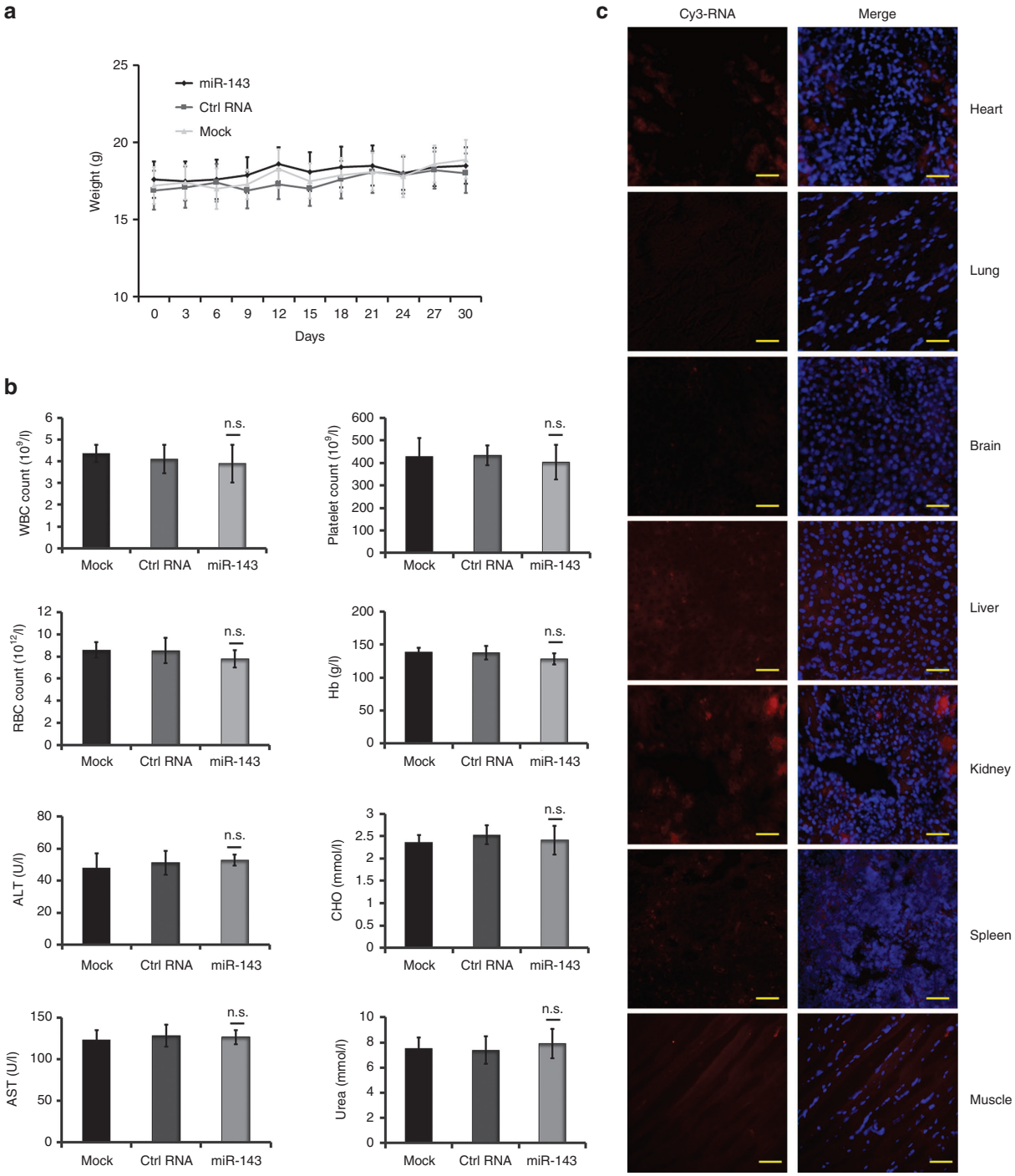


**Figure 5 Toxicity analyses following intravenous delivery of encapsulated miRNA agomir in triple-negative breast cancer (TNBC) xenografts.** Another three randomized groups of TNBC tumor-bearing xenografts were established ($n = 3$ mice in each group). When tumor diameters reached ~5 mm, encapsulated miRNA agomirs were administered by tail vein injection at 1.5 mg/kg of body weight every 3 days for 10 cycles. (**a**) Body weights were measured every 3 days throughout the study. (**b**) Routine blood tests and biochemical tests were performed in normal BALB/c athymic nude mice after treatment with 1.5 mg/kg of body weight miR-143 agomir or Ctrl RNA agomir or phosphate buffered saline (PBS). (**c**) Cy3 signals were examined in heart, lung, brain, liver, kidney, spleen, muscle tissue slices shown in the left panels to evaluate the biodistribution of Cy3-labeled miR-143 agomir. The merged images with 4′,6-diamidino-2-phenylindole nucleus counterstained are shown in the right panels. Scale bars: 50 μm. Data are presented as mean ± SD.

to an increased level of tumoral necrosis and indicate that [18]F-FDG uptake, particularly the SUVmean, is not a good indicator of tumor proliferation under these circumstances. Additionally, Chodosh *et al.*[31] recommended that oncogenic pathway activation within a tumor, in preference to the rate of proliferation is a dependable predictor of [18]F-FDG uptake

levels. Overall, our results suggest that $^{18}$F-FDG PET/CT can be used to monitor the response of TNBC to miR-143-based therapeutics by targeting tumor glycolysis and for the specific evaluation of cancer therapy through molecular imaging method.

While progress has been made toward targeting metabolic enzymes for cancer therapy, concerns related to the unacceptable effects on normal cells have been raised.[32] Although the biodistribution of miR-143 formulation was not restricted to tumors when administrated systemically, but in other normal organs, which might inhibit HK2 in both tumors and normal tissues, we reason that tumor cells are the main targets of this agent because initially, compared with the relatively high expression in limited normal adult tissues, such as adipose tissues, skeletal muscles, and the heart, HK2 is expressed at much higher levels in extensive tumor tissues.[33] Furthermore, the HK1 isoform, which is structurally and functionally similar to HK2, is ubiquitously expressed in most normal adult tissues and may play a compensatory or redundant role in the absence of HK2, while the myocardium and skeletal muscle may utilize fatty acids as an alternate energy substrate as a buffer.[26] Additionally, as observed in our study, when administered at the same dose and frequency, miR-143 had minimal toxic effects on normal cells.

In summary, we demonstrated that systemic delivery of miR-143 agomir is an effective anticancer strategy for targeting tumor metabolism in TNBCs. Given the link between miR-143 and HK2, $^{18}$F-FDG PET/CT represents an attractive approach for monitoring the response to miR-143-based therapy. Extensive analyses are required to settle the problem of targeting property and unique strategies for evaluation efficacy through molecular imaging approaches requires further exploration.

## Materials and methods

*Cell culture and transfection.* The human breast cancer cell line MDA-MB-231 was obtained from the American Type Culture Collection (ATCC, Manassas, VA), and the cells were cultured at 37°C, 5% $CO_2$ in Dulbecco's modified essential medium supplemented with 10% fetal bovine serum and 1% penicillin/streptomycin. miR-143 mimic and scrambled negative control RNA (Ctrl RNA) were obtained from RiboBio (Guangzhou, China).Transfection was performed using Lipofectamine 2000 (Invitrogen, Carlsbad, CA) according to the manufacturer's instructions. For transfection of the RNA oligonucleotides, 50 nmol/l miR-143 mimic and 50 nmol/l Ctrl RNA were used. Analyses of the effects of miR-143 mimic on recipient cells were performed 24–96 hours after transfection.

*RNA isolation and reverse-transcriptase-polymerase chain reaction assays.* Total RNA was extracted using TRIzol (Invitrogen) and was reverse-transcribed with PrimeScript RT reagent (Takara, Shiga, Japan). The cDNA product was added to a mixture of SYBR Premix Ex Taq II (Takara) along with HK2 forward and reverse primers (5′-AAGG CTTCAAGGCATCTG-3′ and 5′-CCACAGGTCATCATAGTT CC-3′, respectively). Polymerase chain reaction was conducted as follows: 95°C for 30 seconds, followed by 40 cycles at 95°C for 3 seconds and 60°C for 34 seconds. Relative HK2 gene expression was analyzed using the Ct method and normalized using glyceraldehyde-3-phosphate dehydrogenase as an endogenous control.

*Cell proliferation, transwell migration, and apoptosis assays.* The following assays were performed as previously described.[16,34] Briefly, 4 hours after transfection with miR-143 mimic or Ctrl RNA, equal numbers of viable MDA-MB-231 cells were seeded into 96-well plates for cell proliferation assays. Cell growth was determined by MTT assays. Experiments were carried out in triplicate. Apoptosis was determined by flow cytometry using a commercially available Annexin V-FITC apoptosis detection kit (Sigma, St. Louis, MO). Cell migration assays were performed in a 24-well transwell plate with 8-μm polyethylene terephthalate membrane filters (Falcon cell culture insert; BD Biosciences, Franklin Lakes, NJ) separating the lower and upper culture chambers. Approximately 10,000 cells were plated in the upper chamber per well in serum-free Dulbecco's modified essential medium. The bottom chamber contained Dulbecco's modified essential medium with 10% fetal bovine serum. Cells were allowed to migrate for 8 hours. After incubation, the filter was removed and nonmigrating cells on the upper side of the filter were detached using a cotton swab. Filters were fixed with 4% formaldehyde for 15 minutes, cells located in the lower filter were stained with 0.1% crystal violet for 20 minutes, and three random fields were counted. Quantification of the results is presented as the mean ± SD.

*Measurement of glucose consumption, lactate production, and in vitro $^{18}$F-FDG uptake.* Glucose consumption and lactate production were analyzed using a glucose assay kit (Sigma) and lactate assay kit (BioVision, Milpitas, CA) as previously described.[16] In the $^{18}$F-FDG uptake assay, MDA-MB-231 cells were cultured in glucose-free medium containing 37 kBq/ml $^{18}$F-FDG. After incubation for different periods of time (30, 60, 90, and 120 minutes), the cells were stringently rinsed in cold PBS and then $^{18}$F-FDG radioactivity was detected using a gamma counter. Protein concentration of each sample was determined using a Bradford protein assay kit (Promega, Madison, WI) with bovine serum albumin as the standard according to the manufacturer's recommendations. Relative $^{18}$F-FDG uptake was normalized according to the respective cell lysate protein concentration.

*Therapeutic experiments in nude mice.* All animal work was performed in accordance with the Guide for the Care and Use of Laboratory Animals (NIH publication nos. 80-23, revised 1996) and in accordance with the institutional ethical guidelines for animal experimentation. Six to eight-week-old female BALB/c athymic nude mice were used for subcutaneous xenografts. Cy3-labeled miR-143 agomir or Cy3-labeled Ctrl RNA agomir was formulated with MaxSuppressor *In Vivo* RNA-LANCEr II, a neutral lipid-based delivery reagent (BIOO Scientific, Austin, TX) according to the manufacturer's instructions. When tumor diameters reached ~5 mm, TNBC tumor-bearing xenografts were randomized into three groups and encapsulated miRNA agomirs were administered intravenously (i.v.) by tail vein injection at 1.5 mg/kg of

body weight every 3 days for 5 cycles. Tumor growth rates were analyzed by measuring tumor length (L) and width (W) every 3 days and by calculating the volume with the formula ($LW^2$)/2. The Cy3-labeled miR-143 agomir and Cy3-labeled Ctrl RNA agomir were commercially synthesized by RiboBio (Guangzhou, China).

*MicroPET/CT imaging of mice.* Mice bearing TNBC xenografts were subjected to $^{18}$F-FDG microPET/CT analysis, performed on an Inveon MM Platform (Siemens, Munich, Germany), on days 0, 5, 10, and 15. The mice were anesthetized with 2% isoflurane in $O_2$ gas for 18F-FDG injection (a single injection of 0.1 ml $^{18}$F-FDG with an activity of 3.7–7.4 MBq via tail vein). At 40 minutes after administration of the tracer injection, the mice were placed prone on the PET scanner bed and were maintained under continuous anesthesia during the study with 1.5% isoflurane in oxygen at 2 l/min. Inveon Acquisition Workplace (Siemens) was used for scanning. Mice were first subjected to a 5-min CT scan and then to a 10-min PET scan. Images were reconstructed using an OSEM3D algorithm followed by MAP or Fast MAP provided by Inveon Acquisition Workplace. The 3D regions of interest were drawn over the entire tumor guided by CT images and tracer uptake was measured using Inveon Research Workplace software. The SUV was calculated as (decay-corrected activity (kBq) per milliliter of tissue volume)/(injected $^{18}$F-FDG activity (kBq)/body mass (g)).

*Toxicity assessment.* Another three randomized groups of TNBC tumor-bearing xenografts were established ($n = 3$ mice in each group) for toxicity assessment. The mice received tail vein injection of encapsulated miRNA agomirs at 1.5 mg/kg of body weight or PBS every 3 days for 10 cycles. The observed term was extended to 30 days, while the other therapeutic conditions were not changed. The activity level, grooming behaviors and mice weight were observed throughout the study. Blood samples of mice were collected on day 30 for further clinical chemical tests to assess changes in relative values including white blood cells counts, red blood cells counts, hemoglobin, platelets counts, alanine aminotransferase, aspartate aminotransferase, urea, and total cholesterol. Afterwards, mice were sacrificed and major organs were resected, molded with optimal cutting temperature compound, and frozen in liquid nitrogen. Frozen sections were cut with 10 μm thickness and stained with 4′,6-diamidino-2-phenylindole. Cy3 signals from heart, lung, brain, liver, kidney, spleen, and muscle were examined by fluorescence microscope to evaluate the biodistribution of miRNA agomirs.

*Western blotting and immunohistochemistry.* Western blotting assays were carried out using standard procedures. The antibody for HK2 was from Cell Signaling Technology (Danvers, MA). Antibodies for horseradish peroxidase-conjugated goat antirabbit IgG and β-actin were from Sigma. Immunohistochemistry for xenografted tumor sections was performed using standard protocols. The dewaxed 5-mm sections were subjected to an antigen-demasking procedure, which involved brief high-temperature heating of the sections immersed in citrate buffer (10 mmol/l, pH 6.0). Endogenous peroxidases were blocked with 0.03% hydrogen peroxide, and nonspecific binding was blocked with 5% normal goat serum in 0.1% Triton X-100, Tris-buffered saline (pH 7.6). Sections were then separately incubated with rabbit monoclonal anti-proliferating cell nuclear antigen, anti-caspase-3, and anti-HK2 antibody (Cell Signaling Technology) for 2 hours at room temperature. After washing with PBS, the sections were incubated with biotinylated secondary antibody, followed by further incubation with the streptavidin–horseradish peroxidase complex. The sections were then immersed in 3,3′-diaminobenzidine for 5–10 minutes, counterstained with 10% Mayer's hematoxylin, dehydrated, and mounted in a crystal mount.

*Statistical analysis.* All results are presented as mean ± SD. The Student's *t*-test was performed to compare the differences between treated groups relative to their paired controls using SPSS 16.0 software (SPSS, Chicago, IL). *P*-values are indicated in the figures above the two groups compared with a value < 0.05 (denoted by *) considered as significant (***$P < 0.001$ and **$P < 0.01$).

**Acknowledgments** The authors declare no conflict of interest. This work was supported by the National Natural Science Foundation of China (NSFC; No. 81271610 and 81471686).

1. Torre, LA, Bray, F, Siegel, RL, Ferlay, J, Lortet-Tieulent, J and Jemal, A (2015). Global cancer statistics, 2012. *CA Cancer J Clin* **65**: 87–108.
2. Carey, L, Winer, E, Viale, G, Cameron, D and Gianni, L (2010). Triple-negative breast cancer: disease entity or title of convenience? *Nat Rev Clin Oncol* **7**: 683–692.
3. Kassam, F, Enright, K, Dent, R, Dranitsaris, G, Myers, J, Flynn, C *et al.* (2009). Survival outcomes for patients with metastatic triple-negative breast cancer: implications for clinical practice and trial design. *Clin Breast Cancer* **9**: 29–33.
4. Lehmann, BD, Bauer, JA, Chen, X, Sanders, ME, Chakravarthy, AB, Shyr, Y *et al.* (2011). Identification of human triple-negative breast cancer subtypes and preclinical models for selection of targeted therapies. *J Clin Invest* **121**: 2750–2767.
5. Hanahan, D and Weinberg, RA (2011). Hallmarks of cancer: the next generation. *Cell* **144**: 646–674.
6. Warburg, O (1956). On the origin of cancer cells. *Science* **123**: 309–314.
7. Cheson, BD (2011). Role of functional imaging in the management of lymphoma. *J Clin Oncol* **29**: 1844–1854.
8. Fuster, D, Duch, J, Paredes, P, Velasco, M, Muñoz, M, Santamaría, G *et al.* (2008). Preoperative staging of large primary breast cancer with [$^{18}$F]fluorodeoxyglucose positron emission tomography/computed tomography compared with conventional imaging procedures. *J Clin Oncol* **26**: 4746–4751.
9. Robey, RB and Hay, N (2006). Mitochondrial hexokinases, novel mediators of the antiapoptotic effects of growth factors and Akt. *Oncogene* **25**: 4683–4696.
10. Patra, KC and Hay, N (2013). Hexokinase 2 as oncotarget. *Oncotarget* **4**: 1862–1863.
11. Bartel, DP (2009). MicroRNAs: target recognition and regulatory functions. *Cell* **136**: 215–233.
12. Ambros, V (2004). The functions of animal microRNAs. *Nature* **431**: 350–355.
13. Chang, YY, Kuo, WH, Hung, JH, Lee, CY, Lee, YH, Chang, YC *et al.* (2015). Deregulated microRNAs in triple-negative breast cancer revealed by deep sequencing. *Mol Cancer* **14**: 36.
14. Kent, OA, Chivukula, RR, Mullendore, M, Wentzel, EA, Feldmann, G, Lee, KH *et al.* (2010). Repression of the miR-143/145 cluster by oncogenic Ras initiates a tumor-promoting feed-forward pathway. *Genes Dev* **24**: 2754–2759.
15. Michael, MZ, O' Connor, SM, van Holst Pellekaan, NG, Young, GP and James, RJ (2003). Reduced accumulation of specific microRNAs in colorectal neoplasia. *Mol Cancer Res* **1**: 882–891.
16. Jiang, S, Zhang, LF, Zhang, HW, Hu, S, Lu, MH, Liang, S *et al.* (2012). A novel miR-155/miR-143 cascade controls glycolysis by regulating hexokinase 2 in breast cancer cells. *EMBO J* **31**: 1985–1998.
17. Peschiaroli, A, Giacobbe, A, Formosa, A, Markert, EK, Bongiorno-Borbone, L, Levine, AJ *et al.* (2013). miR-143 regulates hexokinase 2 expression in cancer cells. *Oncogene* **32**: 797–802.
18. Fang, R, Xiao, T, Fang, Z, Sun, Y, Li, F, Gao, Y *et al.* (2012). MicroRNA-143 (miR-143) regulates cancer glycolysis via targeting hexokinase 2 gene. *J Biol Chem* **287**: 23227–23235.
19. Gregersen, LH, Jacobsen, A, Frankel, LB, Wen, J, Krogh, A and Lund, AH (2012). MicroRNA-143 down-regulates Hexokinase 2 in colon cancer cells. *BMC Cancer* **12**: 232.
20. Yoshino, H, Enokida, H, Itesako, T, Kojima, S, Kinoshita, T, Tatarano, S *et al.* (2013). Tumor-suppressive microRNA-143/145 cluster targets hexokinase-2 in renal cell carcinoma. *Cancer Sci* **104**: 1567–1574.

21. Yao, M, Wang, X, Tang, Y, Zhang, W, Cui, B, Liu, Q *et al.* (2014). Dicer mediating the expression of miR-143 and miR-155 regulates hexokinase II associated cellular response to hypoxia. *Am J Physiol Lung Cell Mol Physiol* **307**: L829–L837.
22. Guo, H, Chen, Y, Hu, X, Qian, G, Ge, S and Zhang, J (2013). The regulation of Toll-like receptor 2 by miR-143 suppresses the invasion and migration of a subset of human colorectal carcinoma cells. *Mol Cancer* **12**: 77.
23. Xu, YF, Li, YQ, Guo, R, He, QM, Ren, XY, Tang, XR *et al.* (2015). Identification of miR-143 as a tumour suppressor in nasopharyngeal carcinoma based on microRNA expression profiling. *Int J Biochem Cell Biol* **61**: 120–128.
24. Mathupala, SP, Ko, YH and Pedersen, PL (2009). Hexokinase-2 bound to mitochondria: cancer's stygian link to the "Warburg Effect" and a pivotal target for effective therapy. *Semin Cancer Biol* **19**: 17–24.
25. Wolf, A, Agnihotri, S, Micallef, J, Mukherjee, J, Sabha, N, Cairns, R *et al.* (2011). Hexokinase 2 is a key mediator of aerobic glycolysis and promotes tumor growth in human glioblastoma multiforme. *J Exp Med* **208**: 313–326.
26. Patra, KC, Wang, Q, Bhaskar, PT, Miller, L, Wang, Z, Wheaton, W *et al.* (2013). Hexokinase 2 is required for tumor initiation and maintenance and its systemic deletion is therapeutic in mouse models of cancer. *Cancer Cell* **24**: 213–228.
27. Zhao, S, Liu, H, Liu, Y, Wu, J, Wang, C, Hou, X *et al.* (2013). miR-143 inhibits glycolysis and depletes stemness of glioblastoma stem-like cells. *Cancer Lett* **333**: 253–260.
28. Selbach, M, Schwanhäusser, B, Thierfelder, N, Fang, Z, Khanin, R and Rajewsky, N (2008). Widespread changes in protein synthesis induced by microRNAs. *Nature* **455**: 58–63.
29. Noguchi, S, Yasui, Y, Iwasaki, J, Kumazaki, M, Yamada, N, Naito, S *et al.* (2013). Replacement treatment with microRNA-143 and -145 induces synergistic inhibition of the growth of human bladder cancer cells by regulating PI3K/Akt and MAPK signaling pathways. *Cancer Lett* **328**: 353–361.
30. Wang, L, Shi, ZM, Jiang, CF, Liu, X, Chen, QD, Qian, X *et al.* (2014). MiR-143 acts as a tumor suppressor by targeting N-RAS and enhances temozolomide-induced apoptosis in glioma. *Oncotarget* **5**: 5416–5427.
31. Alvarez, JV, Belka, GK, Pan, TC, Chen, CC, Blankemeyer, E, Alavi, A *et al.* (2014). Oncogene pathway activation in mammary tumors dictates FDG-PET uptake. *Cancer Res* **74**: 7583–7598.
32. Vander Heiden, MG (2011). Targeting cancer metabolism: a therapeutic window opens. *Nat Rev Drug Discov* **10**: 671–684.
33. Wilson, JE (2003). Isozymes of mammalian hexokinase: structure, subcellular localization and metabolic function. *J Exp Biol* **206**(Pt 12): 2049–2057.
34. Jiang, S, Zhang, HW, Lu, MH, He, XH, Li, Y, Gu, H *et al.* (2010). MicroRNA-155 functions as an OncomiR in breast cancer by targeting the suppressor of cytokine signaling 1 gene. *Cancer Res* **70**: 3119–3127.